Spatial Policy: Guiding Visuomotor Robotic Manipulation with Spatial-Aware Modeling and Reasoning

Yijun Liu[1], Yuwei Liu[2], Yuan Meng[1], Jieheng Zhang[3], Yuwei Zhou[1], Ye Li[1], Jiacheng Jiang[1], Kangye Ji[1], Shijia Ge[1], Zhi Wang[1], Wenwu Zhu[1]

[1]Tsinghua University
[2]Beijing University of Technology
[3]Guangzhou University

Abstract

Vision-centric hierarchical embodied models have demonstrated strong potential for long-horizon robotic control. However, existing methods lack spatial awareness capabilities, limiting their effectiveness in bridging visual plans to actionable control in complex environments. To address this problem, we propose Spatial Policy (SP), a unified spatial-aware visuomotor robotic manipulation framework via explicit spatial modeling and reasoning. Specifically, we first design a spatial-conditioned embodied video generation module to model spatially guided predictions through a spatial plan table. Then, we propose a spatial-based action prediction module to infer executable actions with coordination. Finally, we propose a spatial reasoning feedback policy to refine the spatial plan table via dual-stage replanning. Extensive experiments show that SP significantly outperforms state-of-the-art baselines, achieving a 33.0% average improvement over the best baseline. With an 86.7% average success rate across 11 diverse tasks, SP substantially enhances the practicality of embodied models for robotic control applications. Code and checkpoints are maintained at https://plantpotatoonmoon.github.io/SpatialPolicy/.

Introduction

In recent years, hierarchical embodied models combining high-level planning and low-level action have achieved remarkable success in long-horizon robotic manipulation (Brohan et al. 2024; Cheang et al. 2024; Ze et al. 2024; Li et al. 2025b). Among these approaches, vision-based methods, known as visuomotor robotic manipulation, have emerged as a particularly promising direction. By leveraging rich visual cues, these methods enable effective cross-hierarchical information transfer across diverse robotic embodiments and environments (Du et al. 2023; Tian et al. 2024; Ko et al. 2023; Soni et al. 2025; Black et al. 2023; Li et al. 2025a). Specicially, visuomotor robotic manipulation employs a generative model to predict trajectories of future video, which are subsequently translated into executable actions through a action prediction module.

Despite significant advances, existing visuomotor robotic manipulation frameworks lack spatial awareness ability, failing to effectively bridge visual plans to executable actions in complex environments (Tian et al. 2024; Black et al. 2023). For instance, AVDC (Ko et al. 2023) lacks explicit spatial modeling in its video generation process, resulting in physically implausible predictions, such as robotic arms passing through walls. Feedback module of CLOVER (Bu et al. 2024) enhances dynamic environment adaptation, but its inability to process spatial relationships prevents handling of occluded target scenarios (Tian et al. 2024).

To tackle this problem, we investigate the spatial-aware visuomotor robotic manipulation via explicit spatial modeling and reasoning, which introduces three key challenges: (1) how to generate videos that explicitly model spatial relations, such as object-goal positioning and task alignment; (2) how to utilize the generated videos to guide action prediction in a way that preserves spatial consistency and task relevance; and (3) how to reason over spatial cues during execution to enable real-time feedback that effectively bridges visual and control.

To address these challenges, we propose Spatial Policy (**SP**), a unified framework for robotic manipulation that integrates spatial-aware video generation, action prediction, and feedback. The core idea is to unify spatial modeling and reasoning via a spatial plan table that guides video generation, enables spatially consistent action prediction, and supports feedback-driven refinement during execution. Specifically, (1) we propose a Spatial-Conditioned Embodied Video Generation module that generates visual predictions guided by a structured spatial plan table, which encodes object-goal relations and directional cues to ensure spatial coherence in imagined futures, addressing the challenge of modeling spatially meaningful video trajectories; (2) we introduce a Spatial-Based Action Prediction module that infers executable actions by capturing spatial motion dynamics between predicted frames using spatial coordinates, tackling the challenge of translating visual predictions into spatially consistent actions; (3) we develop a Spatial Reasoning Feedback Policy that refines the spatial plan and video execution through dual-stage replanning based on VLM feedback and rule-based corrections, solving the challenge of real-time spatial reasoning during policy execution. Extensive experiments demonstrate that our model outperforms existing baselines, achieving 86.7% performance. The contributions of this paper are summarized as follows:

- **Spatial policy for vision-action alignment.** We propose SP, a spatially grounded visuomotor policy framework that explicitly models and reasons about spatial struc-

tures to align visual prediction with executable actions.

- **Modular design with structured spatial modeling and reasoning.** SP consists of three synergistic modules: a spatial-conditioned video generation module guided by a structured spatial plan table, a spatial-based action prediction that preserves spatial consistency, and a spatial reasoning feedback policy that refines execution through real-time spatial replanning.
- **Comprehensive evaluation and strong performance.** We conduct extensive experiments on the MetaWorld benchmark to assess the impact of spatial integration, including ablations on video generation, action prediction, and feedback mechanisms. SP outperforms prior methods by over 30%, demonstrating the effectiveness of spatial reasoning in visuomotor robotic manipulation.

Related Work

Video Generation for Embodied Manipulation

Video generation has recently been explored as a visual planning mechanism for embodied agents. AVDC (Ko et al. 2023) generates action-annotated video plans from raw RGB inputs using dense correspondencesenabling policy learning without action supervision. However, due to the lack of explicit spatial reasoning in both generation and action prediction, limiting precision in manipulation tasks. VideoAgent (Soni et al. 2025) refines video plans via self-conditioning to reduce hallucinations and improve visual quality. However, it inherits the lack of explicit spatial reasoning from AVDC in both generation and action prediction, limiting precision in geometry-sensitive manipulation tasks. Clover (Bu et al. 2024) introduces a closed-loop framework combining video diffusion planning and feedback control via an embedding-based error signal, achieving strong results in long-horizon tasks. However, its spatial modeling is limited to depth-based cues and lacks explicit 3D spatial planning or structured geometric reasoning, which restricts generalization across diverse spatial layout. SEER (Tian et al. 2024)proposes a Predictive Inverse Dynamics Model (PIDM) that forecasts future visual states and infers actions end-to-end, closing the loop between vision and control. While it achieves strong performance through large-scale training, it lacks explicit spatial reasoning modules and does not leverage structured spatial plans, which may limit interpretability and adaptability in geometry-sensitive tasks. SuSIE (Black et al. 2023) leverages an image-editing diffusion model to generate visual subgoals for a low-level goal-conditioned policy, enabling better generalization in unstructured environments. However, its subgoal generation relies on appearance-based edits without explicit incorporation of 3D spatial relationships, limiting its precision in spatially complex manipulation scenarios.

Spatial Reasoning in Vision-Language Embodied Systems

Spatial understanding has been addressed in embodied AI from several perspectives. SpatialVLM (Chen et al. 2024a) and GraspCorrect (Lee, Hong, and Kim 2025) leverage pretrained vision-language models to extract chain-of-thought spatial cues and determine object relations in manipulation tasks. 3D-VLA (Zhen et al. 2024) explicitly encodes spatial semantics by aligning 3D vision with textual instructions. SPA (Zhu et al. 2025) utilizes point cloud reconstruction for spatial alignment in manipulation and navigation tasks. Meanwhile, LLM-Planner (Song et al. 2023)and related methods employ large language models to infer spatially structured plans in symbolic form.

Despite these advances, such methods either focus on semantic spatial understanding or operate in symbolic domains, lacking visual feedback and executable rollout. Moreover, most rely on handcrafted prompts or static spatial priors and do not support continuous video generation. In contrast, our work closes this gap by embedding structured spatial plans—automatically derived from environment geometry—into a generative video prediction framework, thereby tightly coupling spatial reasoning and visual synthesis for action-aware planning.

Spatial Conditioning in Generative Video Models

Recent advances in text-to-video diffusion models, such as AnimateDiff (Guo et al. 2024) and VideoCrafter2 (Chen et al. 2024b), achieve high-fidelity generation but lack controllability over agent behavior or scene dynamics. ScenarioDiff (Zhang et al. 2025) and DirecT2V (Hong et al. 2024) propose spatially guided generation using manually specified constraints like bounding boxes or motion paths. These constraints are often synthetic and decoupled from real embodied agent states, limiting their adaptability and semantic alignment with embodied control tasks.

Spatial Policy

We propose a visuomotor robotic manipulation framework that integrates structured spatial reasoning into the perception-to-control pipeline, enabling robots to generate spatially consistent visual plans and execute them reliably. As illustrated in Fig. 1, our system comprises three interconnected modules. First, the **Spatial-Conditioned Embodied Video Generation** module generates future video trajectories conditioned on a structured spatial plan table composed of atomic actions, directional vectors, and relative distances. Second, the **Spatial-Based Action Prediction** module predicts actions aligned with the generated video using the spatial coordinates. Third, the **Spatial Reasoning Feedback Policy** monitors spatial alignment during execution and dynamically refines both the spatial plan table and the visual predictions. Together, these modules form a closed-loop framework that maintains spatial consistency across video imagination, action prediction, and feedback-based reasoning.

Spatial Conditioned Embodied Video Generation

To generate spatially grounded visual trajectories for visuomotor robotic manipulation, we adopt a conditional diffusion framework for future video prediction. The model takes as input an initial observation frame and a textual task description, and generates a sequence of future frames representing high-level visual plans. To enhance spatial aware-

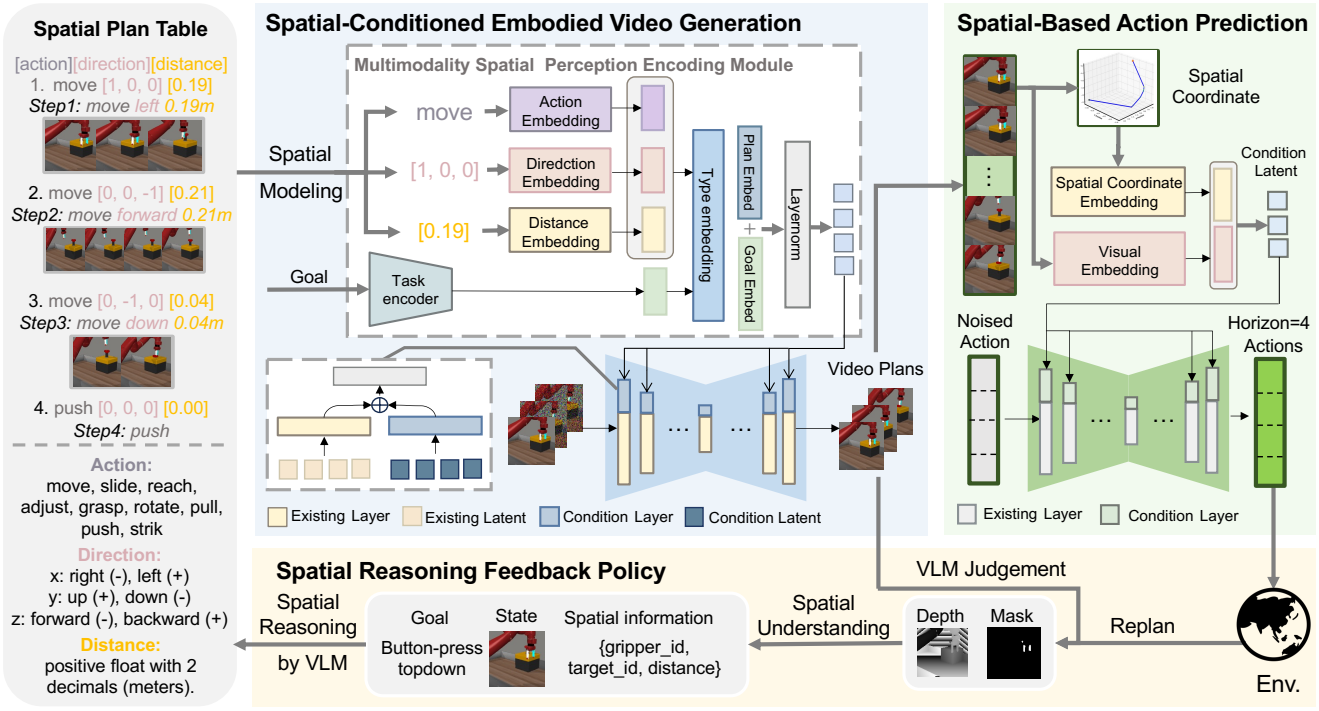

Figure 1: **Framework Overview of Spatial Policy.** Our system comprises three modules: (1) **Spatial-Conditioned Embodied Video Generation**, which uses a **Spatial Plan Table** obtained via VLM reasoning over the spatial offset between the robot and the object, to guide diffusion model in generating spatially coherent video prediction. (2) **Spatial-Based Action Prediction**, which converts the generated video into executable actions using spatial coordinates. (3) **Spatial Reasoning Feedback Policy**, which enables real-time correction via a dual-stage replanning strategy, combining VLM-based video judgement and policy diagnostics to refine the spatial plan table for closed-loop control.

ness, we additionally introduce spatial plan table derived from spatial relationships as an auxiliary global condition.

Spatial Plan Table To capture precise spatial intent, we extract the coordinates of the robot end-effector $\mathbf{p}_{\text{ee}} \in \mathbb{R}^3$ and the target object $\mathbf{p}_{\text{obj}} \in \mathbb{R}^3$ from the simulator, and compute their relative offset as $\Delta\mathbf{p} = \mathbf{p}_{\text{obj}} - \mathbf{p}_{\text{ee}}$. This spatial offset is passed into a pretrained visual-language model (GPT-4o) to produce a structured spatial plan. The generated plan consists of sequential subgoals, each encoding an atomic action with an action type, a direction vector, and a distance scalar, as illustrated in Fig. 1.

Encoding and Integration Each subgoal is independently encoded into a fixed-dimensional latent vector. Concretely, the action type is mapped to an embedding $\mathbf{e}_{\text{act}} \in \mathbb{R}^d$ via a learnable embedding table, the direction vector is discretized and embedded into $\mathbf{e}_{\text{dir}} \in \mathbb{R}^d$ using another learnable embedding table, and the distance scalar is projected into $\mathbf{e}_{\text{dis}} \in \mathbb{R}^d$ through a learnable MLP. The combined subgoal embedding is given by:

$$\mathbf{e}_{\text{subplan}} = \text{MLP}\left([\mathbf{e}_{\text{act}}; \mathbf{e}_{\text{dir}}; \mathbf{e}_{\text{dis}}]\right), \tag{1}$$

All subgoal embeddings $\{\mathbf{e}_1, \ldots, \mathbf{e}_n\}$ are concatenated with the task text embedding $\mathbf{z}_{\text{task}} \in \mathbb{R}^d$ obtained via CLIP (Radford et al. 2021) to form the composite global condition:

$$\mathcal{T} = [\mathbf{z}_{\text{task}}; \mathbf{e}_1; \ldots; \mathbf{e}_n]. \tag{2}$$

This global condition is injected into all layers of the u-net through conditional normalization mechanisms, guiding the diffusion model to produce spatially grounded, instruction-aligned video sequences.

Conditional Diffusion Formulation We follow the design of a u-net-based denoising diffusion probabilistic model, adapted from the Imagen architecture (Ho et al. 2022), consistent with AVDC (Ko et al. 2023). Given an initial frame $\mathbf{I}_0 \in \mathbb{R}^{H\times W\times 3}$ and a composite condition vector $\mathcal{T}$ that incorporates both task instructions and structured spatial information, the model predicts a sequence of $T = 7$ future frames $\mathbf{I}_{1:T}$, resulting in an 8-frame trajectory. The generative objective is to approximate the posterior distribution:

$$p(\mathbf{I}_{1:T} \mid \mathbf{I}_0, \mathcal{T}), \tag{3}$$

where the training target is to denoise a Gaussian-perturbed version of the future frames. Specifically, the model mini-

mizes the following mean squared error (MSE) loss:

$$\mathcal{L}_{\text{MSE}} = \mathbb{E}_{\epsilon,t} \left\| \epsilon - \epsilon_\theta \left(\sqrt{1-\beta_t} \cdot \mathbf{I}_{1:T} + \sqrt{\beta_t} \cdot \epsilon,\, t \mid \mathbf{I}_0, \mathcal{T} \right) \right\|^2, \tag{4}$$

where $\epsilon \sim \mathcal{N}(0, \mathbf{I})$ is sampled noise, β_t is the diffusion schedule, and ϵ_θ is the model's denoising network. Further training details are provided in the Appendix.

Spatial Based Action Prediction

To convert spatially grounded visual plans into executable actions, we design an Spatial Coordinate-Guided Action Prediction module built upon the diffusion policy framework (Chi et al. 2023; Ji et al. 2025), due to its strong capacity for modeling multimodal distributions and complex temporal dependencies, making it particularly well-suited for capturing the spatial variability and uncertainty inherent in visual planning. The model predicts multi-step actions that guide the robot from the current observation toward the visual goal implicitly defined by the generated video sequence, leveraging spatial coordinate to capture fine-grained spatiotemporal dynamics.

Multimodal Spatial Input Encoding We condition our policy on three types of information: (1) the current image $\mathbf{I}_{\text{cur}}$, (2) the goal image $\mathbf{I}_{\text{goal}}$ (sampled from the generated visual plan within the next k steps, i.e., $\mathbf{I}_{\text{goal}} = \mathbf{I}_{t+\delta}$ where $1 \leq \delta \leq k$), and (3) the spatial coordinate of robotic arms $\mathbf{p}_{\text{cur}} \in \mathbb{R}^3$. These inputs capture both spatial and temporal motion cues. All inputs are encoded into compact feature vectors: the image pair is stacked along the channel dimension and passed through a shared ResNet encoder, while the spatial coordinate is encoded via a shallow MLP. The resulting modality-specific features are then concatenated to form a unified condition vector, which guides the denoising network in our diffusion policy-based action prediction model.

Diffusion Policy-based Action Prediction Model We formulate action prediction as a conditional generative process. Specifically, we adopt a unet-based diffusion policy architecture to model the conditional distribution over action trajectories:

$$p_\theta(\mathbf{a}_{0:H-1} \mid \mathbf{I}_{\text{cur}}, \mathbf{I}_{\text{goal}}, \mathbf{p}_{\text{cur}}) \tag{5}$$

where $\mathbf{a}_{0:H-1}$ denotes a sequence of H actions, each including a 3-DoF end-effector pose and gripper control. We train the policy via denoising score matching, minimizing:

$$\mathcal{L}_{\text{MSE}} = \mathbb{E}_{\mathbf{a},\epsilon,t} \left\| \epsilon - \epsilon_\theta \left(\sqrt{1-\beta_t} \cdot \mathbf{a} + \sqrt{\beta_t} \cdot \epsilon, t \mid \mathbf{c} \right) \right\|^2 \tag{6}$$

where $\mathbf{c}$ denotes the concatenated global condition vector from all encoded inputs, $\epsilon \sim \mathcal{N}(0, \mathbf{I})$ is Gaussian noise, and t is the diffusion timestep. ϵ_θ is the learned denoising network. At inference time, the model predicts the entire action trajectory in a denoising pass, and the resulting sequence is executed step-by-step in the environment. Further training details are provided in the Appendix.

Spatial Reasoning Feedback Policy

To ensure spatial consistency throughout execution, we introduce a Spatial Reasoning Feedback Policy that enables closed-loop correction by dynamically refining the Spatial Plan Table based on perceptual feedback. This module integrates a dual-stage feedback mechanism, operating at both the video validation and action execution levels.

During visual planning, we incorporate a vision-language model (VLM)-based consistency checker inspired by VideoAgent (Soni et al. 2025). A pretrained GPT-4o model is prompted to assess the spatial plausibility of the generated video—verifying object-goal alignment, manipulator trajectories, and overall spatial coherence. Only videos that pass this check are used for downstream control; otherwise, regeneration is triggered under the same spatial condition.

During action execution, we employ rule-based policy diagnostics to monitor temporal progress and detect failures such as positional drift or behavioral stagnation. When triggered, the system computes an updated spatial offset between the end-effector and the target object based on the latest observation. This offset is re-encoded into a refined spatial subplan via GPT-4o, forming an updated condition to replan both the video and action policy.

Through this real-time refinement of spatial intent and control guidance, our system maintains alignment between visual imagination and robotic execution, enabling robust long-horizon manipulation.

Experiments

Datasets and Experimental Setups

Datasets and Environments. We follow the evaluation setup of (Ko et al. 2023) and conduct experiments in the Meta-World (Yu et al. 2020). Meta-World is a simulated benchmark designed for assessing robotic manipulation capabilities, consisting of 11 representative single-arm tasks (such as pushing, pulling, grasping, and inserting) performed by a Sawyer robotic arm. We run 25 random seeds across 11 tasks and 3 camera views, yielding over 800 rollouts in total, and evaluate 5 ablation studies in our model.

Baselines and Our Methods

- **AVDC**: A two-stage control planning framework is employed, wherein a pretrained diffusion-based generative model synthesizes a video sequence, followed by the estimation of inter-frame motion using an optical flow network. The resulting motion is then used to inversely infer the corresponding action sequence.
- **AVDC-Replan**: An extension of AVDC that incorporates a replanning mechanism. During execution, if action failure or robotic arm stagnation is detected, a new video is regenerated and a revised action plan is inferred.
- **VideoAgent**: This method employs a self-supervised consistency mechanism to iteratively refine the generated video. Multiple candidate video plans are scored using GPT-4, and the most promising one is selected for execution.
- **VideoAgent-online-Replan**: An extension of VideoAgent that continuously collects successful execution trajectories during deployment. These are used to update both the video generation and optimization models online. A replanning strategy is also introduced to regenerate videos when execution failures occur.

Method	door-open	door-close	basketball	shelf-place	btn-press	btn-press-top
AVDC	30.7%	28.0%	21.3%	8.0%	34.7%	17.3%
AVDC-R	72.0%	89.3%	37.3%	18.7%	60.0%	24.0%
VA	40.0%	29.3%	13.3%	9.3%	38.7%	18.7%
VA-OR	82.7%	97.3%	40.0%	26.7%	73.3%	44.0%
SP	**98.6%**	**100.0%**	66.7%	80.0%	94.7%	96.0%
SP-R	**98.6%**	**100.0%**	**73.3%**	**92.0%**	**96.0%**	**98.6%**

Method	faucet-close	faucet-open	handle-press	hammer	assembly	**Overall**
AVDC	12.0%	17.3%	41.3%	0.0%	5.3%	19.6%
AVDC-R	53.3%	24.0%	81.3%	8.0%	6.7%	43.1%
VA	46.7%	12.0%	36.0%	0.0%	1.3%	22.3%
VA-OR	74.7%	46.7%	86.7%	8.0%	10.7%	53.7%
SP	**93.3%**	89.3%	**100.0%**	**74.7%**	24.0%	83.4%
SP-R	92.0%	**96.0%**	**100.0%**	73.3%	**32.0%**	**86.7%**

Table 1: Comparison of task success rates (%) across 11 MetaWorld tasks. Each method is evaluated over 800 episodes per task. **R** denotes variants equipped with a replanning mechanism. **OR** indicates methods that combine online reinforcement learning with replanning. Bold indicates best.

- **SP (Ours)**: We extract structured planning information from spatial context using VLM, and inject it into the diffusion model via global condition to effectively guide video generation. The generated video is subsequently translated into executable actions using a goal-conditioned policy.
- **SP-Replan (Ours)**: An extended version of our method that performs iterative video generation in the planning phase. During execution, if robotic arm stagnation is detected, a new video is regenerated and the action sequence is re-inferred.

Main Results

As shown in Table 1, our method achieves a success rate of 83.4% without requiring execution-time replanning, already outperforming all prior baselines. In contrast, methods such as AVDC and VA rely on task text to generate videos or pretrained optical flow to compute displacement coordinates for action prediction. These baselines are fragile during deployment, once a deviation or unexpected event occurs, they must fall back on explicit replanning to recover; otherwise, the robot stalls. By contrast, our approach leverages spatial plans to generate structured, goal-aligned videos and predicts executable actions that inherently adapt to spatial variations, leading to more robust and consistent task completion. SP-R further boosts performance to 86.7%, demonstrating the effectiveness of incorporating real-time spatial reasoning into the control loop.

On the subset of challenging tasks (*Assembly, Hammer, Faucet Open, Button Press Top, Shelf Place, and Basketball*), our method achieves an average success rate of 77.5%, significantly outperforming the best-performing baseline, which only reaches 29.2% . This corresponds to a relative improvement of 165.4%. On simpler tasks, our approach achieves near-perfect performance, often approaching 100% success.

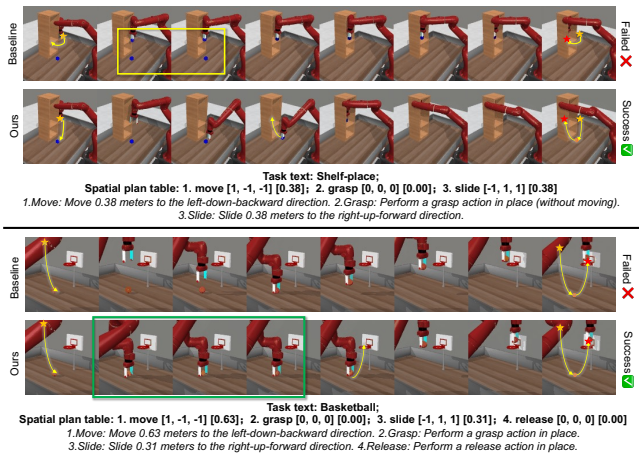

Figure 2: Comparative visualization of spatial planning and video generation results for two representative tasks: *Shelf Place* and *Basketball*. The **yellow line** depicts the motion trajectory; the ★ symbol marks the initial position, the ★ symbol indicates the final task position, and the ● symbols denote intermediate steps along the path.

In the *Shelf Place* task, as shown in Figure 2, the baseline method generates an incorrect and inflexible trajectory (highlighted in the yellow box), resulting in task failure due to its inability to adapt to environmental variations. In contrast, our approach, enhanced with spatial understanding, enables the robotic arm to follow a dynamically planned path and successfully complete the placement task. Similarly, in the *Basketball* task (also illustrated in Figure 2), our method exhibits refined spatial reasoning by allocating more frames (highlighted in the green box) around the critical manipu-

lation event—grasping the ball—leading to smoother and more precise motions. The baseline method, lacking this focused spatial adaptation, often misses essential interaction moments. These results underscore the benefits of integrating spatial awareness with dynamic feedback for robust and effective long-horizon robotic planning.

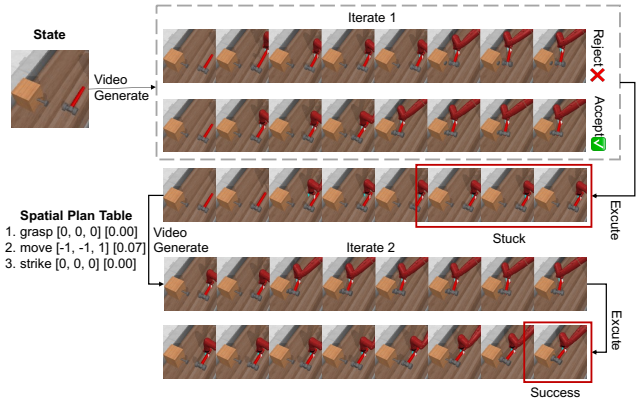

Figure 3: Visualization of the replanning-based spatial planning process for a manipulation task.

Figure 3 further demonstrates how our method leverages spatial feedback and iterative replanning to recover from failures and achieve successful task execution. Unlike baseline planning, which can fail when the initial path is invalid, our approach dynamically adapts, resulting in more robust and reliable performance.

Ablation Study

Ablations on the Video Generation Model. We compare three strategies in the video generation module to evaluate their impact on video quality and downstream control performance. (1) The baseline uses AVDC's video generation approach, where a diffusion model is conditioned only on task text and the initial frame. (2) The *Distance* variant directly encodes the spatial offset between the robot and target object (spatial coordinates) and concatenates it with the task prompt as input. (3) The *Subplan* variant leverages a vision-language model to transform spatial coordinates into structured subplans that encode action type, direction, and distance, which are then injected into the diffusion model.

As shown in Table 2, both spatial variants outperform the AVDC baseline, demonstrating the *utility of explicitly modeling spatial structures for enhanced visuomotor performance*. Moreover, the subplan-based approach achieves further gains by abstracting raw spatial cues into structured guidance, highlighting the *importance of structured spatial abstraction in facilitating precise and actionable visual plan generation*.

Ablations on the Action Prediction Model. AVDC uses a pre-trained flow model to estimate pixel-wise motion between the current and goal frames, then converts the flow into a spatial target coordinate. The robot executes actions using a classical controller to move toward the point and applies gripper control based on heuristics. In contrast, our method is built on diffusion policy and directly predicts executable actions from the current frame, goal frame, and robot spatial coordinates. This design captures spatial and temporal context jointly and allows flexible adaptation to unexpected events such as object shifts or failures. Results in Table 3 show that our approach achieves higher success rates and better robustness, confirming that *learning-based spatial reasoning provides more effective action prediction than coordinate-based control*.

	Easy	Medium	Hard	Very Hard	**Overall**
AVDC	75.0%	48.7%	**26.7%**	48.0%	63.4%
Distance	93.5%	56.7%	25.3%	**81.3%**	79.4%
Subplan	**96.8%**	**63.3%**	24.0%	78.7%	**82.4%**

Table 2: Comparison of task success rates (%) using different video generation strategies across four levels of task difficulty. **AVDC** uses text and initial frame only; **Distance** adds raw spatial offsets; **Subplan** injects structured spatial subplans.

	Easy	Medium	Hard	Very Hard	**Overall**
Flow	25.9%	10.7%	5.3%	8.0%	19.6%
Ours	**75.0%**	**48.7%**	**26.7%**	**48.0%**	**63.4%**

Table 3: Comparison of task success rates (%) between our method and AVDC's action prediction module across four levels of task difficulty. **Flow** denotes the flow model-based action prediction used in AVDC; **Ours** denotes our spatial-based action prediction module.

Ablation on Spatial Condition Injection Strategy in Video Generation. To investigate how spatial conditions affect video generation, we conduct an ablation study comparing two injection strategies for integrating the spatial plan table into the diffusion model. (1) The spatial plan table is concatenated with the task embedding and propagated uniformly across all layers of the U-Net backbone in the *Global Cond* variant directly. This approach provides consistent spatial guidance throughout the generation process. (2) Inspired by GLIGEN (Li et al. 2023), the spatial plan is injected only into intermediate U-Net layers via a cross-attention mechanism in the *Local Cond* variant, allowing localized spatial modulation while preserving the task-level prompt as a global condition.

Both strategies are trained under identical configurations and evaluated on MetaWorld. As shown in Table 4, Local Conditioning slightly improves the average task success rate and shows better performance on harder tasks (e.g., +5.3% on Hard). These results suggest that *injecting spatial structure via localized attention can enhance spatial precision during video synthesis, thereby improving policy success rates, especially in more challenging environments*.

Ablations on the Replanning Mechanism. We compare three settings to evaluate the effect of the replanning mechanism: (1) no replanning at all, (2) replanning only during the

	Easy	Medium	Hard	Very Hard	**Overall**
Global Cond	96.8%	**63.3%**	24.0%	78.7%	82.4%
Local Cond	**99.0%**	62.0%	**29.3%**	**80.0%**	**84.3%**

Table 4: Comparison of task success rates (%) using different spatial condition injection strategies for video generation across four levels of task difficulty. **Global Cond** injects the spatial plan table across all U-Net blocks; **Local Cond** follows GLIGEN-style partial injection via cross-attention at intermediate layers.

	Easy	Medium	Hard	Very Hard	**Overall**
NR	96.8%	63.3%	24.0%	78.7%	82.4%
GR	96.0%	70.7%	24.0%	80.0%	83.4%
GR&ER	**97.3%**	**73.3%**	**32.0%**	**92.0%**	**86.7%**

Table 5: Comparison of task success rates (%) using different replanning mechanisms across four levels of task difficulty. **NR** denotes no replanning; **GR** denotes generation replanning; **ER** denotes execution replanning. Bold indicates best.

video generation stage, and (3) replanning during both the video generation and real execution stages. As shown in Table 5, task success improves when replanning is introduced.

Our experiments demonstrate that enabling replanning during both the imagination and real execution stages significantly enhances task success by facilitating dynamic adaptation to the evolving environment. While replanning solely during the imagination stage offers limited improvements, the integration of a vision-language-based evaluation module allows the system to selectively regenerate and retain higher-quality trajectories, effectively filtering out suboptimal predictions despite the inherent stochasticity of video generation. Without any replanning, the model's performance deteriorates due to its inability to recover from unforeseen variations. Therefore, *a combined replanning strategy is crucial for achieving robust and effective long-horizon robotic control*.

Ablations on Finetuning with Additional Execution Data. To assess the impact of trajectory diversity on policy robustness, we compare two training data configurations for our model. (1) The model is trained exclusively on demonstrations where tasks are completed successfully from start to finish without failure. (2) The model is further finetuned on an expanded dataset that includes recovery trajectories where execution initially failed but eventually succeeded when resumed from intermediate states.

Finetuning on these recovery trajectories yields noticeable gains, particularly on challenging tasks. On *btn-press-top*, the success rate improves from 97.3% to 99.0%. More strikingly, on the more complex *hammer* task, performance increases from 68.0% to 78.7%. These results indicate that *including partial-to-successful executions enhances the model's robustness by exposing it to diverse recovery scenarios*. Such data enables better generalization to states not frequently seen in the original dataset of consistently successful trials.

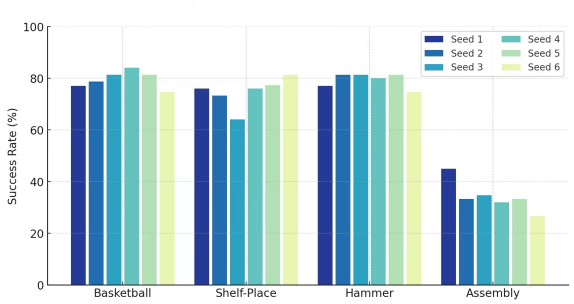

Figure 4: Task success rates on four challenging MetaWorld tasks under different diffusion noise seeds using our SP method, demonstrating consistent performance across seeds.

Hyperparameter Analysis

Effect of Diffusion Noise Seed in Video Generation. To assess the robustness of our video generation module under different stochastic conditions, we conduct experiments using our proposed method (SP) on four challenging Meta-World tasks: *basketball*, *shelf-place*, *hammer*, and *assembly*. For each task, we sample six different diffusion noise seeds and report the task success rates. As shown in Figure 4, our approach consistently achieves high performance across seeds, with an average success rate around 77% and low variance. This indicates that the structured spatial subplans effectively anchor the generation process, ensuring the production of reliable and executable visual trajectories even under varying random conditions.

Effect of Hyperparameter in Action Prediction. We analyze key design choices in the action prediction module. First, we study the effect of goal frame selection range. Setting the goal frame as a random future frame within the next $k = 20$ timesteps yields over 10% higher average success rates compared to restricting it to a narrower window between 17–20 timesteps ahead, indicating that allowing a broader temporal horizon improves generalization and task adaptability. Second, regressing the noise ϵ achieves better performance than directly predicting the denoised action $\hat{a}_0$, which contrasts with some prior findings (Chi et al. 2023). Lastly, while direct MLP-based action regression converges faster, the diffusion-based denoising model demonstrates superior performance and robustness across tasks.

Conclusion

We present **SP**, a spatial-aware visuomotor framework that integrates explicit spatial modeling and reasoning into robot manipulation. Central to our approach is a spatial plan table that encodes atomic actions, directions, and distances, enabling structured spatial guidance throughout the pipeline. Our polciy generates spatially coherent visual trajectories by conditioning a video diffusion model on spatial plan table, , which are then used to guide action prediction based on

temporally aligned spatial coordinates. A dual-stage replanning mechanism enhances spatial reasoning by refining the spatial plan table and regenerating video and actions upon inconsistency, ensuring closed-loop correction. Experiments on MetaWorld show that SP improves success rates by over 33% compared to prior methods, validating the effectiveness of spatial modeling and reasoning.

References

Black, K.; Nakamoto, M.; Atreya, P.; Walke, H.; Finn, C.; Kumar, A.; and Levine, S. 2023. Zero-shot robotic manipulation with pretrained image-editing diffusion models. *arXiv preprint arXiv:2310.10639*.

Brohan, A.; Brown, N.; Chebotar, Y.; Chen, X.; Choromanski, K.; Ding, T.; Driess, D.; Dubey, A.; Finn, C.; Florence, P.; Fu, C.; Arenas, M.; Gopalakrishnan, K.; Han, K.; Hausman, K.; Herzog, A.; Hsu, J.; Ichter, B.; Irpan, A.; Joshi, N.; Julian, R.; Kalashnikov, D.; Kuang, Y.; Leal, I.; Lee, L.; Lee, T.-W.; Levine, S.; Lu, Y.; Michalewski, H.; Mordatch, I.; Pertsch, K.; Rao, K.; Reymann, K.; Ryoo, M.; Salazar, G.; Sanketi, P.; Sermanet, P.; Singh, J.; Singh, A.; Soricut, R.; Tran, H.; Vanhoucke, V.; Vuong, Q.; Wahid, A.; Welker, S.; Wohlhart, P.; Wu, J.; Xia, F.; Xiao, T.; Xu, P.; Xu, S.; Yu, T.; and Zitkovich, B. 2024. RT-2: Vision-Language-Action Models Transfer Web Knowledge to Robotic Control.

Bu, Q.; Zeng, J.; Chen, L.; Yang, Y.; Zhou, G.; Yan, J.; Luo, P.; Cui, H.; Ma, Y.; and Li, H. 2024. Closed-loop visuomotor control with generative expectation for robotic manipulation. *Advances in Neural Information Processing Systems*, 37: 139002–139029.

Cheang, C.-L.; Chen, G.; Jing, Y.; Kong, T.; Li, H.; Li, Y.; Liu, Y.; Wu, H.; Xu, J.; Yang, Y.; et al. 2024. Gr-2: A generative video-language-action model with web-scale knowledge for robot manipulation. *arXiv preprint arXiv:2410.06158*.

Chen, B.; Xu, Z.; Kirmani, S.; Ichter, B.; Driess, D.; Florence, P.; Sadigh, D.; Guibas, L.; and Xia, F. 2024a. SpatialVLM: Endowing Vision-Language Models with Spatial Reasoning Capabilities. *arXiv preprint arXiv:2401.12168*.

Chen, H.; Zhang, Y.; Cun, X.; Xia, M.; Wang, X.; Weng, C.; and Shan, Y. 2024b. VideoCrafter2: Overcoming Data Limitations for High-Quality Video Diffusion Models. *arXiv preprint arXiv:2401.09047*.

Chi, C.; Xu, Z.; Feng, S.; Cousineau, E.; Du, Y.; Burchfiel, B.; Tedrake, R.; and Song, S. 2023. Diffusion policy: Visuomotor policy learning via action diffusion. *The International Journal of Robotics Research*, 02783649241273668.

Deng, J.; Dong, W.; Socher, R.; Li, L.-J.; Li, K.; and Fei-Fei, L. 2009. ImageNet: A large-scale hierarchical image database. *IEEE Conference on Computer Vision and Pattern Recognition (CVPR)*, 248–255.

Du, Y.; Yang, S.; Dai, B.; Dai, H.; Nachum, O.; Tenenbaum, J.; Schuurmans, D.; and Abbeel, P. 2023. Learning universal policies via text-guided video generation. *Advances in neural information processing systems*, 36: 9156–9172.

Farnebäck, G. 2003. Two-frame motion estimation based on polynomial expansion. In *Scandinavian Conference on Image Analysis*, 363–370. Springer.

Guo, Y.; Yang, C.; Rao, A.; Liang, Z.; Wang, Y.; Qiao, Y.; Agrawala, M.; Lin, D.; and Dai, B. 2024. AnimateDiff: Animate Your Personalized Text-to-Image Diffusion Models without Specific Tuning. *arXiv preprint arXiv:2307.04725*.

He, K.; Zhang, X.; Ren, S.; and Sun, J. 2016. Deep Residual Learning for Image Recognition. In *Proceedings of the IEEE Conference on Computer Vision and Pattern Recognition (CVPR)*, 770–778.

Ho, J.; Chan, W.; Saharia, C.; Whang, J.; Gao, R.; Gritsenko, A.; Kingma, D. P.; Poole, B.; Norouzi, M.; Fleet, D. J.; et al. 2022. Imagen video: High definition video generation with diffusion models. *arXiv preprint arXiv:2210.02303*.

Hong, S.; Seo, J.; Shin, H.; Hong, S.; and Kim, S. 2024. DirecT2V: Large Language Models are Frame-Level Directors for Zero-Shot Text-to-Video Generation. *arXiv preprint arXiv:2305.14330*.

Ji, K.; Meng, Y.; Cui, H.; Li, Y.; Hua, S.; Chen, L.; and Wang, Z. 2025. Block-wise Adaptive Caching for Accelerating Diffusion Policy. *arXiv preprint arXiv:2506.13456*.

Ko, P.-C.; Mao, J.; Du, Y.; Sun, S.-H.; and Tenenbaum, J. B. 2023. Learning to act from actionless videos through dense correspondences. *arXiv preprint arXiv:2310.08576*.

Lee, S.; Hong, Y.; and Kim, K. I. 2025. GraspCorrect: Robotic Grasp Correction via Vision-Language Model-Guided Feedback. *arXiv preprint arXiv:2503.15035*.

Li, P.; Wu, H.; Huang, Y.; Cheang, C.; Wang, L.; and Kong, T. 2025a. Gr-mg: Leveraging partially-annotated data via multi-modal goal-conditioned policy. *IEEE Robotics and Automation Letters*.

Li, Y.; Liu, H.; Wu, Q.; Mu, F.; Yang, J.; Gao, J.; Li, C.; and Lee, Y. J. 2023. Gligen: Open-set grounded text-to-image generation. In *Proceedings of the IEEE/CVF conference on computer vision and pattern recognition*, 22511–22521.

Li, Y.; Meng, Y.; Sun, Z.; Ji, K.; Tang, C.; Fan, J.; Ma, X.; Xia, S.; Wang, Z.; and Zhu, W. 2025b. SP-VLA: A Joint Model Scheduling and Token Pruning Approach for VLA Model Acceleration. *arXiv preprint arXiv:2506.12723*.

Loshchilov, I.; and Hutter, F. 2019. Decoupled Weight Decay Regularization. In *International Conference on Learning Representations (ICLR)*.

Lowe, D. G. 2004. Distinctive image features from scale-invariant keypoints. *International Journal of Computer Vision*, 60(2): 91–110.

Radford, A.; Kim, J. W.; Hallacy, C.; Ramesh, A.; Goh, G.; Agarwal, S.; Sastry, G.; Askell, A.; Mishkin, P.; Clark, J.; et al. 2021. Learning transferable visual models from natural language supervision. In *International conference on machine learning*, 8748–8763. PmLR.

Song, C. H.; Wu, J.; Washington, C.; Sadler, B. M.; Chao, W.-L.; and Su, Y. 2023. LLM-Planner: Few-Shot Grounded Planning for Embodied Agents with Large Language Models. *arXiv preprint arXiv:2212.04088*.

Soni, A.; Venkataraman, S.; Chandra, A.; Fischmeister, S.; Liang, P.; Dai, B.; and Yang, S. 2025. VideoAgent: Self-Improving Video Generation for Embodied Planning. In *Workshop on Reinforcement Learning Beyond Rewards@ Reinforcement Learning Conference*.

Tian, Y.; Yang, S.; Zeng, J.; Wang, P.; Lin, D.; Dong, H.; and Pang, J. 2024. Predictive inverse dynamics models are scalable learners for robotic manipulation. *arXiv preprint arXiv:2412.15109*.

Wang, Z.; Bovik, A. C.; Sheikh, H. R.; and Simoncelli, E. P. 2004. Image quality assessment: from error visibility to structural similarity. *IEEE Transactions on Image Processing*, 13(4): 600–612.

Yu, T.; Quillen, D.; He, Z.; Julian, R.; Hausman, K.; Finn, C.; and Levine, S. 2020. Meta-world: A benchmark and evaluation for multi-task and meta reinforcement learning. In *Conference on robot learning*, 1094–1100. PMLR.

Ze, Y.; Zhang, G.; Zhang, K.; Hu, C.; Wang, M.; and Xu, H. 2024. 3d diffusion policy: Generalizable visuomotor policy learning via simple 3d representations. *arXiv preprint arXiv:2403.03954*.

Zhang, Y.; Wang, X.; Chen, H.; Qin, C.; Hao, Y.; Mei, H.; and Zhu, W. 2025. ScenarioDiff: Text-to-video Generation with Dynamic Transformations of Scene Conditions. *International Journal of Computer Vision*, 133: 4909–4922.

Zhen, H.; Qiu, X.; Chen, P.; Yang, J.; Yan, X.; Du, Y.; Hong, Y.; and Gan, C. 2024. 3D-VLA: A 3D Vision-Language-Action Generative World Model. *arXiv preprint arXiv:2403.09631*.

Zhu, H.; Yang, H.; Wang, Y.; Yang, J.; Wang, L.; and He, T. 2025. SPA: 3D Spatial-Awareness Enables Effective Embodied Representation. *arXiv preprint arXiv:2410.08208*.

Inference Pipeline

As shown in alg. 1, Our inference process consists of three stages: spatial-conditioned embodied video generation, spatial-based action prediction, and spatial reasoning feedback policy. Given an initial observation and the current spatial coordinates of the robot and object, we compute a relative spatial offset $\Delta\mathbf{p}$, which is used to generate a spatial plan table via a VLM. The spatial plan table is fused with the task prompt and fed into a diffusion video generator to produce a goal-directed visual trajectory.

To infer executable actions, the action prediction model takes the predicted video sequence and encodes the current spatial state, represented solely by the robot end effector coordinate $\mathbf{p}_{\text{ee}}$, through a learnable MLP. This enables precise grounding of actions in the spatial context. During execution, a feedback module monitors task progress. If stagnation is detected, a two stage replanning mechanism is triggered: the spatial plan table is refined, and a new video and action sequence are generated to resume progress. This pipeline enables real time, spatially consistent decision making under dynamic conditions.

Training Details: Video Generation and Action Prediction

Video Generation

Training Settings. All models are trained on 128×128 RGB frames sampled as 8-frame clips. We use the AdamW optimizer (Loshchilov and Hutter 2019) with an initial learning rate of 1×10^{-4} and a cosine learning rate schedule. Training is conducted for 100,000 steps, unless otherwise specified. The standard batch size is 8 for training and 16 for validation, with gradient accumulation set to 1. Mixed precision training is employed using FP16 and automatic mixed precision (AMP). A linear diffusion noise schedule is used with $\beta_1 = 1 \times 10^{-4}$ and $\beta_T = 0.02$ over 1000 steps. Exponential Moving Average (EMA) with a decay factor of 0.999 is updated every 10 training steps. Conditional dropout with a probability of 0.1 is applied to all models except the Baseline. Validation uses 1 or 2 samples per batch depending on the script. Unless otherwise specified, all training datasets are collected and generated from our own single successful executions. All experiments are conducted on a single NVIDIA RTX 4090 GPU (80GB memory), with full-precision (FP32) training completed within 2 days.

Inference. During inference, all models use DDIM sampling with classifier-free guidance. Models conditioned on plans demonstrate improved semantic consistency and object interaction fidelity.

Model Variants and Conditioning. We investigate four variants of our conditional diffusion models, differing mainly in conditioning inputs and architectural enhancements. Key differences and training datasets are summarized in Table 6.

Action Prediction

Training Settings. Unlike the original Diffusion Policy (Chi et al. 2023), which conditions on past observations and actions, our model relies solely on the current observation, future observation, and spatial context. Specifically, instead of using a standard 3-channel RGB input, we concatenate the current frame and a sampled goal frame to form a 6-channel input image of resolution 128×128, along with spatial coordinates. Given horizon $H = 4$, the model predicts H future actions from a single observation step ($T = 1$), conditioned on the current frame, spatial coordinates, and a goal frame sampled within the next $K = 20$ frames. We adopt a ResNet-50 visual encoder (He et al. 2016) pretrained on ImageNet (Deng et al. 2009), which remains trainable during training. The spatial coordinates are encoded via a MLP, which is also trained end-to-end. The policy network is implemented as a conditional U-Net with diffusion denoising, using a cosine noise schedule ($\beta_1 = 1 \times 10^{-4}$, $\beta_T = 2 \times 10^{-2}$) over 100 steps. The model is optimized using AdamW with learning rate $\eta = 1 \times 10^{-4}$, weight decay 1×10^{-6}, and batch size $B = 512$ for both training and validation. The learning rate follows a cosine annealing schedule with 500 warm-up steps. Exponential Moving Average (EMA) is applied with a maximum decay rate of

Algorithm 1: Inference Pipeline

Input: Environment $\mathcal{E}$, Task prompt $\mathcal{T}_0$, Policy π
Output: Success flag $\mathcal{S}$
$\mathbf{I}_0 \leftarrow \mathcal{E}.\texttt{Render}(),\ (\mathbf{p}_{\text{ee}}, \mathbf{p}_{\text{obj}}) \leftarrow \mathcal{E}.\texttt{GetSpatialState}()$;
$\mathcal{S}_0 \leftarrow \texttt{GPT4o}(\Delta\mathbf{p} = \mathbf{p}_{\text{obj}} - \mathbf{p}_{\text{ee}}),\ \mathcal{T} \leftarrow [\mathcal{T}_0; \mathcal{S}_0]$;
repeat
  $\mathbf{V}_{1:T} \leftarrow \texttt{DiffusionGenerate}(\mathbf{I}_0, \mathcal{T})$
until *VLMCheck*$(\mathbf{V}_{1:T})$ *succeeds*;
$\mathbf{z}_{\text{coord}} \leftarrow \texttt{EncodeCoord}(\mathbf{p}_{\text{ee}}, \mathbf{p}_{\text{obj}}),\quad \mathcal{A}_{1:H} \leftarrow \pi(\mathbf{V}_{1:T}, \mathbf{z}_{\text{coord}})$;
for $t = 1$ **to** H **do**
  $\mathcal{E}.\texttt{Step}(\mathcal{A}_t)$;
  if *IsStuck*$(\mathcal{E})$ **then**
    $\mathbf{I}_t \leftarrow \mathcal{E}.\texttt{Render}(),\ (\mathbf{p}_{\text{ee}}, \mathbf{p}_{\text{obj}}) \leftarrow \mathcal{E}.\texttt{GetSpatialState}(),\ \mathcal{S}_t \leftarrow \texttt{GPT4o}(\Delta\mathbf{p}),\ \mathcal{T}_t \leftarrow [\mathcal{T}_0; \mathcal{S}_t]$;
    repeat
      $\mathbf{V}_{1:T} \leftarrow \texttt{DiffusionGenerate}(\mathbf{I}_t, \mathcal{T}_t)$
    until *VLMCheck*$(\mathbf{V}_{1:T})$ *succeeds*;
    $\mathbf{z}_{\text{coord}} \leftarrow \texttt{EncodeCoord}(\mathbf{p}_{\text{ee}}, \mathbf{p}_{\text{obj}}),\quad \mathcal{A}_{1:H} \leftarrow \pi(\mathbf{V}_{1:T}, \mathbf{z}_{\text{coord}})$;
$\mathcal{S} \leftarrow \mathcal{E}.\texttt{CheckSuccess}()$;
return $\mathcal{S}$

Version	Description
Baseline (Global Conditioning on Task)	Standard UNet conditioned on global CLIP text embedding, serving as a task-aware video prior.
Global Conditioning on Task & Distance	Adds a 9-dimensional gripper-object distance vector encoder for enhanced spatial grounding.
Global Conditioning on Task & Subplan	Incorporates structured multi-step action plans as global conditioning signals.
Global Conditioning on Task & Subplan (Fine-tuned)	Initially trained on expert data for 10k steps, then fine-tuned on additional datasets for 2k steps.
Local Conditioning on Task & Subplan	Introduces cross-attention to fuse global and local plan features for fine-grained temporal conditioning.

Table 6: Comparison of video generation model variants highlighting key architectural or training differences.

0.9999 to stabilize training. All experiments are conducted on a single NVIDIA RTX 4090 GPU (40GB memory), with full-precision (FP32) training completed within 3 days.

Inference. During inference, we adopt DDIM sampling with classifier-free guidance to generate action sequences. Conditioning on spatial plans significantly enhances semantic alignment and spatial fidelity, leading to more coherent and goal-directed behaviors.

Tasks in Meta-World

In the Meta-World benchmark (Yu et al. 2020), we evaluated the performance on 11 representative robotic manipulation tasks shown in Figure 5, which are designed to assess various manipulation skills and generalization abilities of reinforcement learning algorithms. These tasks are categorized by their difficulty levels as follows:

- **Very Hard:** *Shelf Place*: The agent must grasp an object and place it onto the target shelf. This task is particularly challenging due to the precision required in both grasping and placing the object accurately on the shelf.
- **Hard:** *Assembly*: The agent grasps the handle position and inserts the ring into the slot to complete assembly. This task requires precise manipulation and coordination of multiple parts.
- **Medium:** *Hammer*: The agent grasps the hammer handle and strikes forward to push the nail in with the hammer head. This task involves force control and spatial accuracy. *Basketball*: The task involves grasping the basketball, lifting it up, moving forward above the hoop, and placing it onto the hoop to complete the task. It requires coordinated movement and spatial awareness.
- **Easy:** *Door Open*: The agent is required to push into the door handle grip area and then pull to open the door. *Door Close*: The agent needs to push into the door handle grip area and then push to close the door. *Button Press*: The agent moves horizontally to the button and pushes it in. *Button Press Topdown*: The agent moves above the button and presses down vertically. *Faucet Close*: The agent moves to the left side of the faucet handle and turns it right to close. *Faucet Open*: The agent moves to the right side of the faucet handle and turns it left to open. *Handle Press*: The agent grasps the handle and presses it downwards.

These tasks cover a range of manipulation skills, including pushing, pulling, grasping, placing, pressing, and turning, and they involve different objects and goals, providing a comprehensive evaluation of the agent's ability to learn and generalize across various manipulation tasks.

Dataset Construction

We construct our dataset from expert demonstrations collected in the Meta-World (Yu et al. 2020) simulator. For each task, successful execution trajectories are recorded and stored as NPZ and PKL files. Each trajectory contains RGB, depth, and mask images at each timestep, along with task metadata such as environment name, frame index, and camera parameters.

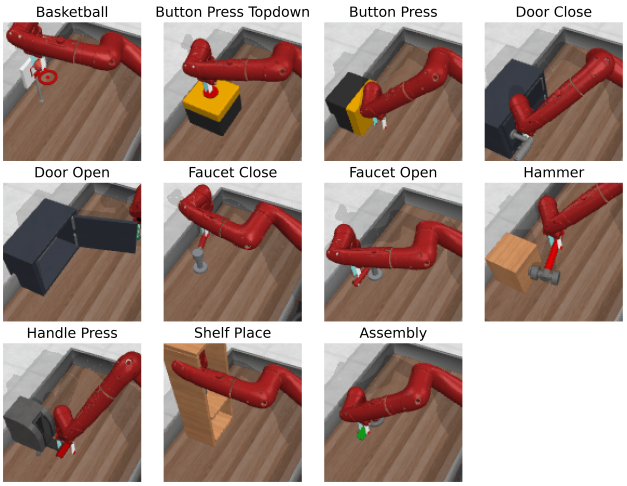

Figure 5: Examples of 11 tasks in meta-world

To enhance the usefulness of the dataset for learning fine-grained control, we identify *fine manipulation intervals* using a spatial-aware strategy. Specifically, we compute the 3D positions of both grippers and task-relevant target points by combining mask and rgb-depth information into point clouds. Distances between grippers and targets are monitored across frames to identify close-contact phases indicative of fine manipulation.

Each raw trajectory is temporally segmented, and frames within fine intervals are sampled at 5× the rate of coarse intervals. The sampling process is governed by the following parameters:

- **Interval:** sampling interval between frames
- **distance_threshold:** maximum distance to consider a frame as fine-grained
- **consecutive frames:** number of consecutive frames required to enter fine-grained phase
- **recovery needed frames:** number of coarse frames required before re-entering fine phase
- **suppress single spike:** whether to ignore short spikes of distance violations
- **max allowed anomaly:** allowed anomaly frames within fine-grained segment

To improve spatial focus, we crop each RGB frame based on task-specific visual layouts. Depending on the task and viewpoint, center or specific regions are retained using manually determined crop windows. The final dataset consists of (1) sampled RGB/mask/depth frames, (2) frame-wise 2D/3D positions of grippers and targets, (3) their pairwise distances, and (4) spatial plan table in textual form.

VLM Prompt Design

We explore the use of vision-language models (VLMs) to provide structured feedback in both generation validation and action refinement. While prior works often use open-ended prompts to guide action planning (e.g., "How should the robot complete this task?"), we find that such free-form task descriptions or scene summaries yield inconsistent or inaccurate responses in our setting.

Ineffective Prompt Types (Abandoned):

- **Task description (ineffective):** Prompts like "close the door slow" or "grasp the basketball carefully" often fail to produce actionable or reliable feedback due to ambiguity and lack of spatial grounding.
- **Scene summary (ineffective):** Descriptions of the visual scene, such as "the door is slightly open, and the gripper is nearby", result in inconsistent VLM interpretation and lack of precise spatial understanding.

Effective Prompt Design: We instead adopt a **structured prompt format** tailored to two specific functionalities shown in Fig. 6:

1. **Video validation (generation filtering):** We use a closed-loop prompt to determine whether a generated video should be accepted or rejected. The prompt emphasizes object completeness and task progression, while tolerating minor visual artifacts. The VLM is instructed to respond with a strict "Accept" or "Reject" based on visual quality.

   This strict, rule-based instruction significantly improves agreement with human judgments, especially in detecting object disappearance or hallucination.

2. **Spatial plan table generation:** As described in Section , we format spatial plan table into structured multi-step plans of the form:

   ```
   Plan:
   1. move [-1, 0, 0] [0.19]
   2. move [0, 0, -1] [0.21]
   3. push [0, 0, 0] [0.00]
   ```

   Each line encodes an action, a direction vector (x: right-/left+, y: up+/down-, z: forward-/back+), and a positive float distance (in meters). These are generated by aligning frame transitions with gripper/target spatial dynamics and then converted into text for conditioning our VLM-enhanced modules.

Conclusion: Our experiments suggest that *free-form prompts are unreliable* for task-level planning or video validation in closed-loop robotic control. Instead, **spatial plan table with explicit roles, response formats, and spatial semantics** lead to significantly more stable and interpretable VLM outputs, which are essential for real-time feedback in visual policy generation.

Frame Matching Mechanism

To ensure precise alignment between visual goals and execution states, we introduce a similarity-based frame matching mechanism. At each timestep, the current observation frame $\mathbf{I}_{\text{cur}}$ is compared to the current target frame $\hat{\mathbf{I}}_g$ sampled from the predicted video sequence $\{\hat{\mathbf{I}}_1, \hat{\mathbf{I}}_2, \ldots, \hat{\mathbf{I}}_K\}$. We compute a composite similarity score via:

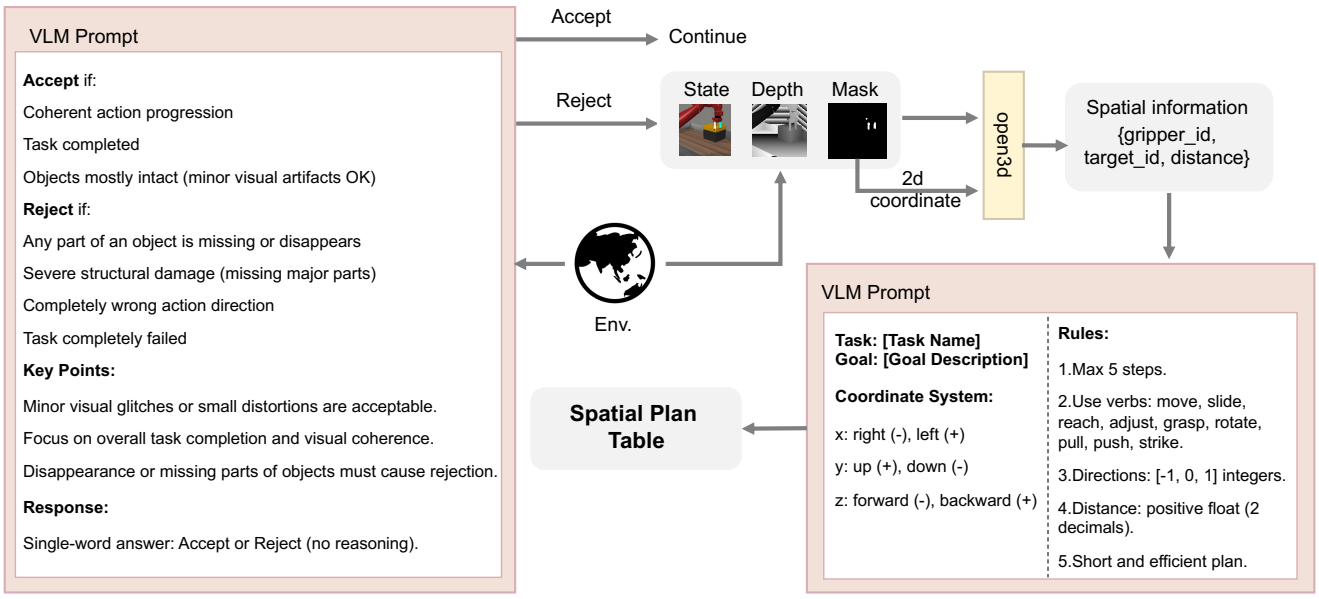

Figure 6: Detailed Design of ours VLM Prompt

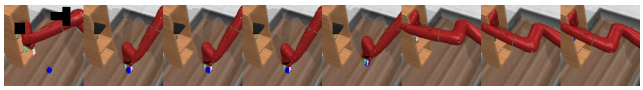

Figure 7: Video generation results with partial occlusion by random masking. Despite masked regions (left), the model generates coherent future frames (right) and maintains correct task execution.

$$\text{Sim}(\mathbf{I}_{\text{cur}}, \hat{\mathbf{I}}_g) = w_{\text{geo}} \cdot \text{Sim}_{\text{geo}} + w_{\text{pos}} \cdot \text{Sim}_{\text{pos}} + w_{\text{ssim}} \cdot \text{SSIM}(\mathbf{I}_{\text{cur}}, \hat{\mathbf{I}}_g) + w_{\text{flow}} \cdot \text{Sim}_{\text{flow}}, \tag{7}$$

where Sim_{geo} is the similarity based on contour and shape features (Lowe 2004), Sim_{pos} encodes block-wise intensity statistics and center-of-mass shifts, SSIM is the structural similarity index between grayscale frames (Wang et al. 2004), and Sim_{flow} measures the inverse magnitude of optical flow (Farnebäck 2003). The weights are set to w_{geo}=0.35, w_{pos}=0.35, w_{ssim}=0.2, and w_{flow}=0.1. A frame is considered matched if:

$$\text{Sim}(\mathbf{I}_{\text{cur}}, \hat{\mathbf{I}}_g) \geq \tau, \tag{8}$$

with the threshold τ=0.8. Upon match, we advance the goal frame to $\hat{\mathbf{I}}_{g+1}$. To prevent deadlocks when similarity fails to exceed the threshold, a hard switch is enforced every T_{max}=28 steps.

Robustness to Occlusions via Masking

To evaluate the robustness of our video generation model under partial visual occlusions, we introduce a masking mechanism before feeding the current frame into the diffusion model. Specifically, we randomly mask a portion of the image input, simulating occlusions such as those caused by environmental factors or sensor noise.

As illustrated in Figure 7, although significant areas of the current frame are masked, the generated frames remain visually consistent and the downstream agent successfully completes the manipulation tasks. This indicates that the model has learned a robust representation of both visual and temporal context, and can infer plausible continuations even when critical input regions are missing.